

# Tooth ultrastructure of a novel COL1A2 mutation expanding its genotypic and phenotypic spectra

Narin Intarak<sup>1</sup>  | Thunyaporn Budsamongkol<sup>1,2</sup>  | Thanakorn Theerapanon<sup>3</sup>  |  
Theerapat Chanamuangkon<sup>4</sup>  | Anucharte Srijunbarl<sup>5</sup>  | Lawan Boonprakong<sup>6</sup>  |  
Thanrira Pornaveetus<sup>1</sup>  | Vorasuk Shotelersuk<sup>7,8</sup> 

<sup>1</sup>Genomics and Precision Dentistry Research Unit, Department of Physiology, Faculty of Dentistry, Chulalongkorn University, Bangkok, Thailand

<sup>2</sup>Geriatric Dentistry and Special Patients Care Program, Faculty of Dentistry, Chulalongkorn University, Bangkok, Thailand

<sup>3</sup>Excellence Center in Regenerative Dentistry, Department of Anatomy, Faculty of Dentistry, Chulalongkorn University, Bangkok, Thailand

<sup>4</sup>Biomaterial Testing Center, Faculty of Dentistry, Chulalongkorn University, Bangkok, Thailand

<sup>5</sup>Dental Materials R&D Center, Faculty of Dentistry, Chulalongkorn University, Bangkok, Thailand

<sup>6</sup>Oral Biology Research Center, Faculty of Dentistry, Chulalongkorn University, Bangkok, Thailand

<sup>7</sup>Center of Excellence for Medical Genomics, Medical Genomics Cluster, Department of Pediatrics, Faculty of Medicine, Chulalongkorn University, Bangkok, Thailand

<sup>8</sup>Excellence Center for Genomics and Precision Medicine, King Chulalongkorn Memorial Hospital, the Thai Red Cross Society, Bangkok, Thailand

## Correspondence

Thanrira Pornaveetus, Genomics and Precision Dentistry Research Unit, Department of Physiology, Faculty of Dentistry, Chulalongkorn University, Bangkok 10330, Thailand.  
Email: thanrira.p@chula.ac.th

## Funding information

This project is funded by National Research Council of Thailand, Global Partnership CU-C16F630029, Health Systems Research Institute, and Thailand Research Fund (MRG6280001, DPG6180001)

## Abstract

**Objectives:** To investigate tooth ultrastructure and mutation of two patients in a family affected with osteogenesis imperfecta (OI) type IV and dentinogenesis imperfecta (DGI).

**Methods:** Mutations were detected by whole exome and Sanger sequencing. The permanent second molar obtained from the proband (DGI1) and the primary first molar from his affected son (DGI2) were studied for their color, roughness, mineral density, hardness, elastic modulus, mineral content, and ultrastructure, compared to the controls.

**Results:** Two novel missense COL1A2 variants, c.752C > T (p.Ser251Phe) and c.758G > T (p.Gly253Val), were identified in both patients. The c.758G > T was predicted to be the causative mutation. Pulp cavities of DGI1 (permanent teeth) were obliterated while those of DGI2 (primary teeth) were wide. The patients' teeth had darker and redder colors; reduced dentin hardness; decreased, disorganized, and scattered dentinal tubules and collagen fibers; and irregular dentinoenamel junction (DEJ), compared to controls. Lacunae-like structures were present in DGI2.

**Conclusions:** We reported the novel causative mutation, c.758G > T (p.Gly253Val), in COL1A2 for OI type IV and DGI. The DGI dentin demonstrated inferior mechanical property and ultrastructure, suggesting severe disturbances of dentin formation. These could contribute to fragility and prone to infection of DGI teeth. This study expands phenotypic and genotypic spectra of COL1A2 mutations.

## KEYWORDS

bisphosphonate, dental disease, dentin, dentinogenesis imperfecta, osteoporosis, skeleton

## 1 | INTRODUCTION

Osteogenesis imperfecta (OI) is a rare heterogeneous inherited disorder of connective tissue with an estimated incidence of 1:15–20,000 individuals (Marini et al., 2017). Main features of OI are bone fragility, deformity, and growth deficiency. Its secondary features include blue sclerae, hearing loss, cardiopulmonary complication, and dentinogenesis imperfecta (DGI). Craniofacial manifestations associated with OI include midfacial hypoplasia, class III malocclusion, and posterior crossbite (O'Connell & Marini, 1999). Irregular pattern and reduced number of dentinal tubules and cracked enamel were reported in DGI teeth (Ibrahim et al., 2019; Wieczorek & Loster, 2013).

OI poses variable severity ranging from perinatal lethality to unnoticeable clinical signs. OI is classically classified into four main types (types I, II, III, and IV) (Sillence et al., 1979). Eighty-five percent of cases are caused by mutations in *COL1A1* or *COL1A2* which encode type I collagen. Of those, substitution of another amino acid for glycine is the most common, causing negative alteration of triple-helical domain of the collagen chains. Mutations in at least 17 other genes in autosomes (Marini et al., 2017) or chromosome X can lead to OI (Lindert et al., 2016). Although many reports have studied mutations in OI patients, knowledge of ultrastructure of DGI teeth is limited.

This study identified the proband and his son affected with type IV OI and DGI. Both patients were found to harbor two novel missense variants, c.752C > T (p.Ser251Phe) and c.758G > T (p.Gly253Val), in *COL1A2*. The teeth affected with DGI obtained from both patients were thoroughly studied for their characteristics including tooth color, roughness, hardness, elastic modulus, mineral density, mineral composition, and ultrastructure.

## 2 | MATERIALS AND METHODS

### 2.1 | Subject enrollment

A Thai family, diagnosed with OI and DGI, enrolled in this study. Informed consents were obtained. The study was approved by the research ethics committee, Faculty of Dentistry, Chulalongkorn University (HREC-DCU 2017-077, date of approval: 6 October 2017) and complied with Declaration of Helsinki (version 2002) and the additional requirements. Medical history was obtained and clinical examination was performed for all participants.

### 2.2 | Mutation analyses

Genomic DNA was isolated from peripheral blood leukocytes and processed by TruSeq Exome Enrichment Kit and Illumina HiSeq 2000 at Macrogen Inc. (Seoul, Korea). The CASAVA v1.7 was used to map the data with the Human Genome version 19 and SAM tools (<http://samtools.sourceforge.net/>) to call variants. The sequencing data were mapped to NCBI37 reference human genome. To exclude polymorphism variants, the identified variants obtained from the subjects were filtered with various databases including NHLBI Exome

Variant Server (EVS), Genome Aggregation Database (gnomAD), 1000 Genomes Project Consortium, dbSNPs and in-house database of 2,166 Thai exomes (including at least 1,000 healthy individuals). The variants located in the coding regions of genes related to osteogenesis imperfecta were screened using the genes listed in OI mutation database (<https://oi.gene.le.ac.uk>). The variants reported here were segregated in affected family members. Mutation pathogenicity was predicted by InterVar (Li & Wang, 2017), Sorting Intolerant From Tolerant (SIFT) (Ng & Henikoff, 2003), and Mendelian Clinically Applicable Pathogenicity (M-CAP) (Jagadeesh et al., 2016).

The identified variant was validated by Sanger sequencing. The coding region of *COL1A2* was amplified using specific primers: F:GTCATGCCACTGTAAGCAAC and R:GCAAACACAGTTCCAATCTTTAC. The amino acid sequence of human *COL1A2* (NP\_000080.2) was compared with that of *Rhesus macaque* (NP\_001253266.1), *Bos taurus* (NP\_776945.1), *Mus musculus* (NP\_031769.2), *Xenopus laevis* (NP\_001080727.1), and *Danio rerio* (NP\_892013.2).

### 2.3 | Tooth samples

The permanent upper left second molar of the proband (DGI1) and the primary lower left first molar of the proband's son (DGI2) were extracted due to caries. DGI teeth were analyzed compared with three tooth type-matched controls collected from healthy age-matched individuals who did not have any systemic condition or medication affecting the teeth and bone.

### 2.4 | Micro computerized tomography (micro-CT)

Tooth samples were scanned with specimen  $\mu$ CT 35 (SCANCO Medical, Brüttsellen, Switzerland) at Faculty of Dentistry, Chulalongkorn University. A square area of 16 00D 16–104x104 pixels from 30 layers of sections was selected from each sample. Mineral density was measured in and quantified using the Image Processing Language (IPL, Scanco Medical AG).

### 2.5 | Tooth color

A digital intraoral colorimeter (ShadeEye NCC Dental Chroma Meter, Shofu Inc., Kyoto, Japan) was used to measure color on buccal and lingual surfaces of tooth crown. The values of colorimeter were demonstrated as  $L^*$ ,  $a^*$ , and  $b^*$ . Color difference ( $\Delta E$  value) between DGI and control teeth was determined following previous study (Alghazali et al., 2012).

### 2.6 | Surface roughness

Surface roughness was examined on the lingual and mesial tooth surfaces using a surface Profilometer (Talyscan 150, Taylor Hobson Ltd., UK). Each surface was measured 30 times randomly at 600

micrometer intervals on y-axis. The stylus speed was 1,000 micrometer/second. Tracing area was  $2 \times 2 \text{ mm}^2$ . Cutoff length was 0.025 mm. The surface topography parameters were calculated by the TalyMap Universal program.

## 2.7 | Nanohardness and elastic modulus

After samples were sectioned, the enamel and dentin were indented using the nano-base indentation system (Ultra Micro-Indentation System, UMIS II, CSIRO, Australia) and a calibrated diamond Berkovich indenter. All samples were indented to maximum force 200 mN for 30 spots. In all loading-unloading cycles, 50 points were plotted to make load-displacement curve. The IBIS software was used to calculate hardness and elastic modulus values.

## 2.8 | Energy-Dispersive X-ray (EDX)

The dehydrated tooth sections were coated with gold powder for 10 s. Mineral contents, carbon (C), oxygen (O), phosphorus (P), and calcium (Ca), in enamel and dentin were measured using EDX (ISIS 300 EDX-system; Oxford Instruments, UK).

## 2.9 | Histology

Samples were subjected to EDTA decalcification, embedded in paraffin wax, sectioned, stained with hematoxylin and eosin and Masson's Trichrome, and examined under light microscope.

## 2.10 | Scanning Electron Microscopy (SEM)

Samples were sputter-coated with gold and examined using SEM (QuantaFeg 250, FEI Company, Oregon, USA).

## 2.11 | Statistical analysis

GraphPad Prism 5 Software Package (GraphPad Software, Inc., San Diego, CA, USA) was used. Data with normal distribution were tested for significance using independent *t* test. Mann-Whitney U test was used for data with non-normal distribution (significance level at 0.05).

# 3 | RESULTS

## 3.1 | Physical and oral characteristics

The proband was a 43-year-old Thai male. He had a history multiple episodes of bone fractures including spontaneous fractures

of his ribs and clavicles at 3 months of age and a fracture of his right femur at age 12 years while jumping. Physical examinations at age 43 years revealed short stature (156 cm; 25th percentile), white sclerae, widen antero-posterior body axis, and marked limb deformities (Figure 1a-c). Radiographic features showed generalized osteopenia, narrow and angulated long bones, hyperlordosis, fish vertebrae, and compression fractures (Figure 1d-g). His BMD of lumbar spine was significantly reduced ( $0.534 \text{ g/cm}^2$ ; z-score  $-3.0$ ). Craniofacial findings included wormian bones, DGI, anterior crossbite, and class III malocclusion. The teeth had severe attrition, marked cervical constriction, and pulp obliteration. Dental radiograph showed bulbous crowns, curved roots, and obliterated pulp canals. The upper left second and third molars were broken and subjected for extraction (Figure 1h-j). He never received pamidronate therapy.

The proband's son was a 3-year-old boy (Figure 2a). He was delivered naturally at 38 weeks of gestation. His birthweight was 2,660 g (25th-50th centile); body length 46 cm (25th centile); head circumference 33 cm (25th-50th centile); and chest circumference 31 cm. He was referred to our hospital due to fracture of his left femur during neonatal period. At 1 month of age, he had right humerus fracture. Callus formation was observed at the left femur and right humerus on the radiographs (Figure 2b,c). Wormian bone formation was found in the lambdoid suture (Figure 2d). The anterior fontanelle was  $5 \times 5 \text{ cm}$ . Intravenous pamidronate ( $7.2 \text{ mg/kg}$ ) was started at the age of 4 months and continued every 2 months. At 5 months of age, his right femur was fractured. Distinct curvature of femurs and humeri and zebra stripe signs were present (Figure 2e-h). His bone age was 3-6 months when his chronological age was 23 months (Figure 2i). Follow-up at age 3 years, he had diffused osteopenia. Callus formation was observed on the left femur and metaphyses of left tibia and fibula. His bone age was 2 years (Figure 2j,k). His lumbar spine BMD was  $0.194 \text{ g/cm}^2$  (z-score  $-0.3$ ) at age 12 months, and  $0.387 \text{ g/cm}^2$  (z-score  $-1.4$ ) at age 36 months (Supplementary Table 1) Serum levels of calcium, phosphate, alkaline phosphatase, thyroid hormones, and insulin-like growth factor were within normal limits. He had triangular face, blue sclerae, and DGI. The teeth showed severe attrition and wide pulp chamber (Figure 2l-o).

## 3.2 | Mutation identification

The proband and his son were diagnosed with OI type IV. WES identified that both harbored two novel missense mutations, c.752C > T (p.Ser251Phe) (ClinVar accession number: SCV001244947) and c.758G > T (p.Gly253Val) (ClinVar accession number: SCV001244948), in exon 16 of the COL1A2 gene (NM\_000089) (Figure 3a-d). Both variants were not present in the databases including the NHLBI Exome Variant Server (EVS), Genome Aggregation Database (gnomAD), 1000 Genomes Project Consortium, and dbSNPs databases. Both COL1A2 variants segregated in the affected individuals including the proband and his son. They were



**FIGURE 1** Clinical and radiographic manifestations of the proband. (a–c) A 43-year-old Thai male with short stature and limb deformities. (d, f) Diffuse osteopenia in the humerus (d), radius and ulna (e), tibia and fibula (f). (g) Hyperlordotic alignment with multiple levels of compression fracture at the thoracic and lumbar spine level. (h) Wormian bones formation in the cranial suture (i) Yellowish opalescent teeth with severe attrition and anterior cross bite. (j) Panoramic radiograph showing bulbous tooth crowns, curved roots, and constriction of pulp canals

not detected in the proband's wife who was healthy. Furthermore, they were not present in 2,166 Thai controls including at least 1,000 healthy individuals. Using *in silico* analyses of variant pathogenicity, the p.Ser251Phe and p.Gly253Val were predicted to be damaging and the residues Ser251 and Gly253 were highly conserved. According to ACMG/AMP 2015 guideline (Richards et al., 2015), the p.Ser251Phe was predicted to be likely pathogenic (PM1, PM2, PP1, PP3) whereas the p.Gly253Val was predicted to be pathogenic (PS1, PS3, PM1, PM2, PP1, PP3). The p.Ser251Phe and p.Gly253Val were predicted to be damaging by SIFT (scores 0.004 and 0.00) (Ng & Henikoff, 2003) and M-CAP (scores 0.042 and 0.913) (Jagadeesh et al., 2016). The residue Ser251 and Gly253 were highly conserved

among species including monkey, cattle, mouse, frog, and zebra fish (Figure 3e).

### 3.3 | Color, surface roughness, and mineral density

The permanent upper left second molar (DG11) and the primary lower left first molar (DG12) were obtained from the proband and proband's son, respectively (Figure 4a and Supplementary Figure 1). The colorimeter detected that the crown of DG11 was darker, redder, and bluer than its controls and DG12 was darker, redder, and yellower than its controls (Supplementary Table 2).

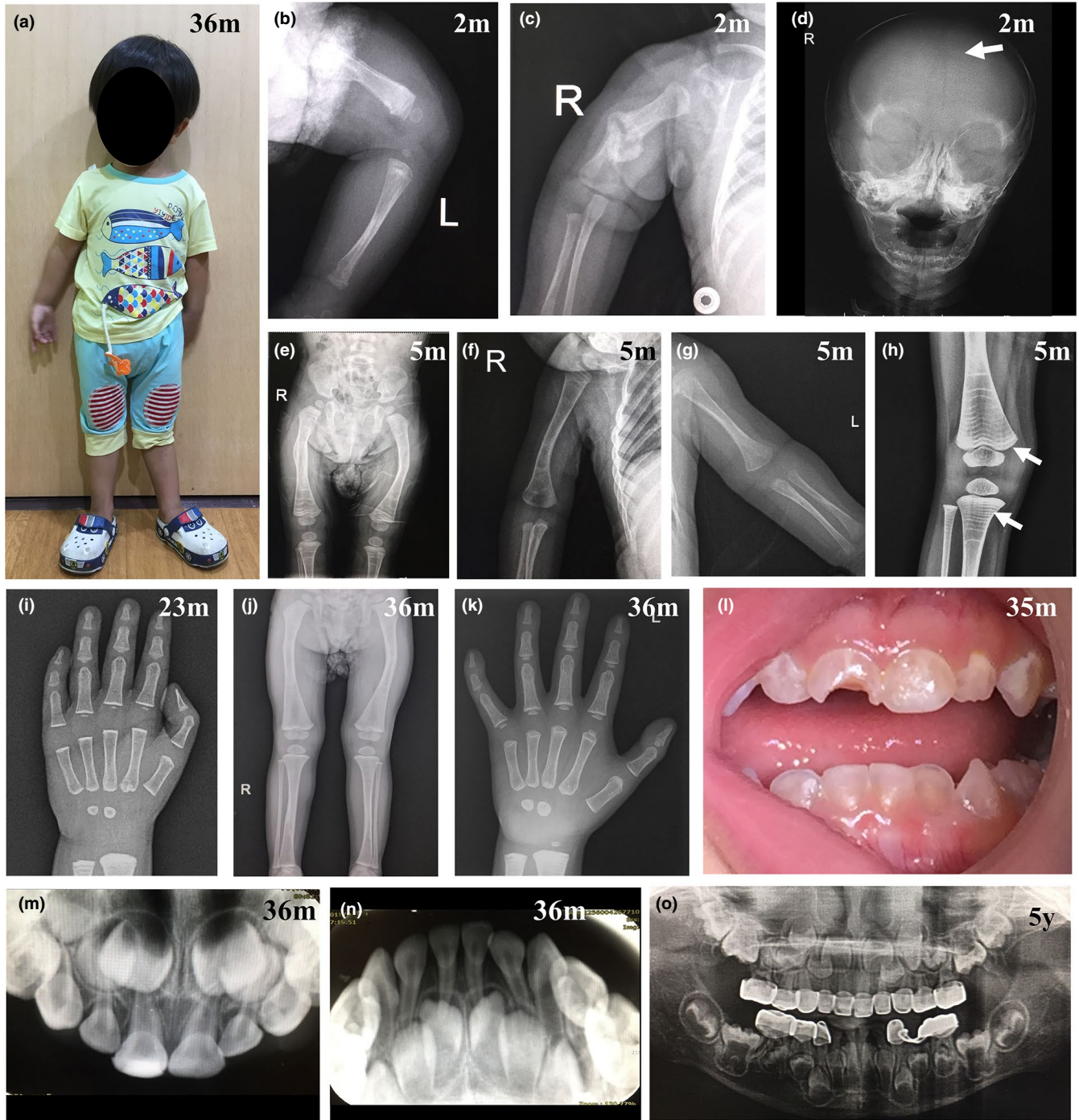


**FIGURE 2** Clinical and radiographic manifestations of the proband's son. (a) A 3-year-old boy with triangular face and deformities of upper thighs. (b, c) Callus formation found in the left femur (b) and right humerus (c). (d) Diffuse osteopenia and wormian bones formation in lambdoid suture of the skull. (e, f) Abnormal curvature of both femurs (e) and right humerus (f). (g) Thin solid periosteal reaction on the left humeral shaft. (h) Zebra stripe sign of pamidronate therapy at the tibia and femur with callus formation at distal metaphyses. (i) Bone age around 3–6 months at chronological age of 23 months. (j) Abnormal curvature of femurs with evidence of callus formation and diffuse osteopenia. (k) Bone age of 24 months at chronological age of 36 months. (l) DGI teeth with severe attrition at age 35 months. (m, n) Radiographs showing wide pulp cavities of primary teeth at age 36 months. (o) Panoramic radiograph at age 5 years showing bulbous crown and wide pulp chamber of teeth. The primary upper anterior and posterior teeth were restored with stainless steel crowns. The chronological age of the patient is shown in the upper right corner

The color difference value ( $\Delta E$ ) between DGI1 and its controls was 10.55, and the  $\Delta E$  between DGI2 and its controls was 11.86. Both  $\Delta E$  values were above 8, which was considered distinctly

perceivable by the human eyes (Yamanel et al., 2010). The surface roughness values of DGI1 and DGI2 were among their controls (Supplementary Figure 2). Micro-CT revealed that the density of

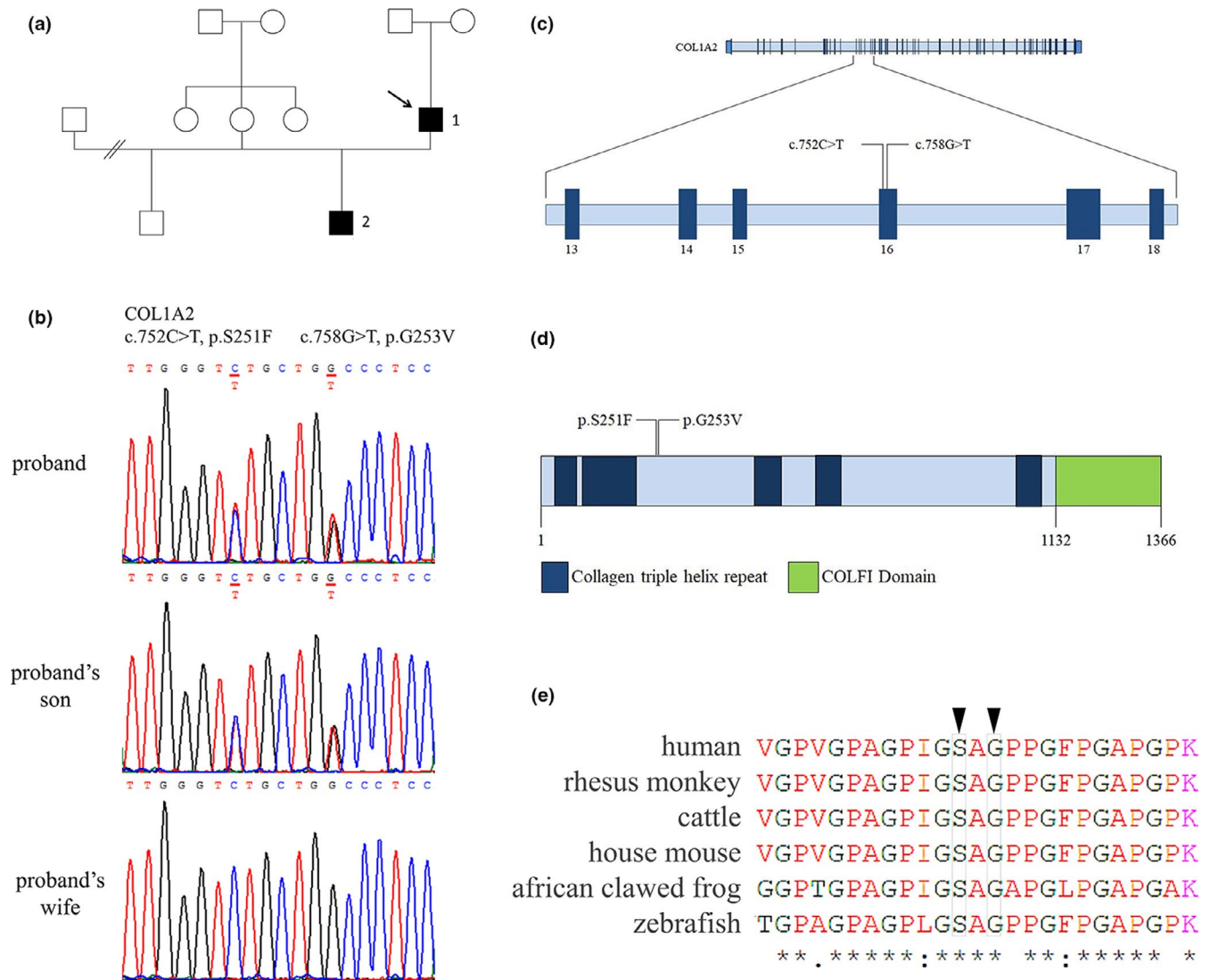


**FIGURE 3** Pedigree of the family and mutation analyses (a) A diagram demonstrates two affected individuals in a non-consanguineous family. The affected patients are denoted in black and the proband is indicated by arrow. (b) Chromatograms of the family show two missense variants in the proband and his son. (c, d) The organization of COL1A2 gene and structural domains of COL1A2 protein indicate the position of mutations. (e) Conservation of the p.Ser251 and p.Gly253 across species are indicated by black arrowheads

DGI1 (both dentin and enamel) was higher than its controls while the density of DGI2 (dentin and enamel) was among its control (Supplementary Table 3).

### 3.4 | Hardness and elastic modulus

The dentin hardness values of both DGI1 and DGI2 were significantly reduced compared to their controls values. DGI1 also showed a significant reduction in enamel hardness compared to its controls while the enamel hardness value of DGI2 was among its control (Figure 4b). Regarding the elastic modulus, a significant decrease was observed in the enamel of DGI1 and the enamel and dentin of DGI2, compared to controls. The elastic modulus of DGI1 dentin was comparable to its controls (Figure 4c).

### 3.5 | Changes in mineral composition

EDX showed that the calcium and phosphorus contents of DGI1 dentin were significantly decreased compared to its controls while those of DGI2 were comparable to its controls. Regarding to the enamel, the mineral contents of both DGI1 and DGI2 were not statistically different from those of their controls (Figure 4d,e).

### 3.6 | Altered tooth ultrastructure

Histologically, DGI1 and DGI2 dentin showed reduced dentinal tubules with non-circular cross section. Longitudinal histological sections showed irregular arrangement of their tubules. In

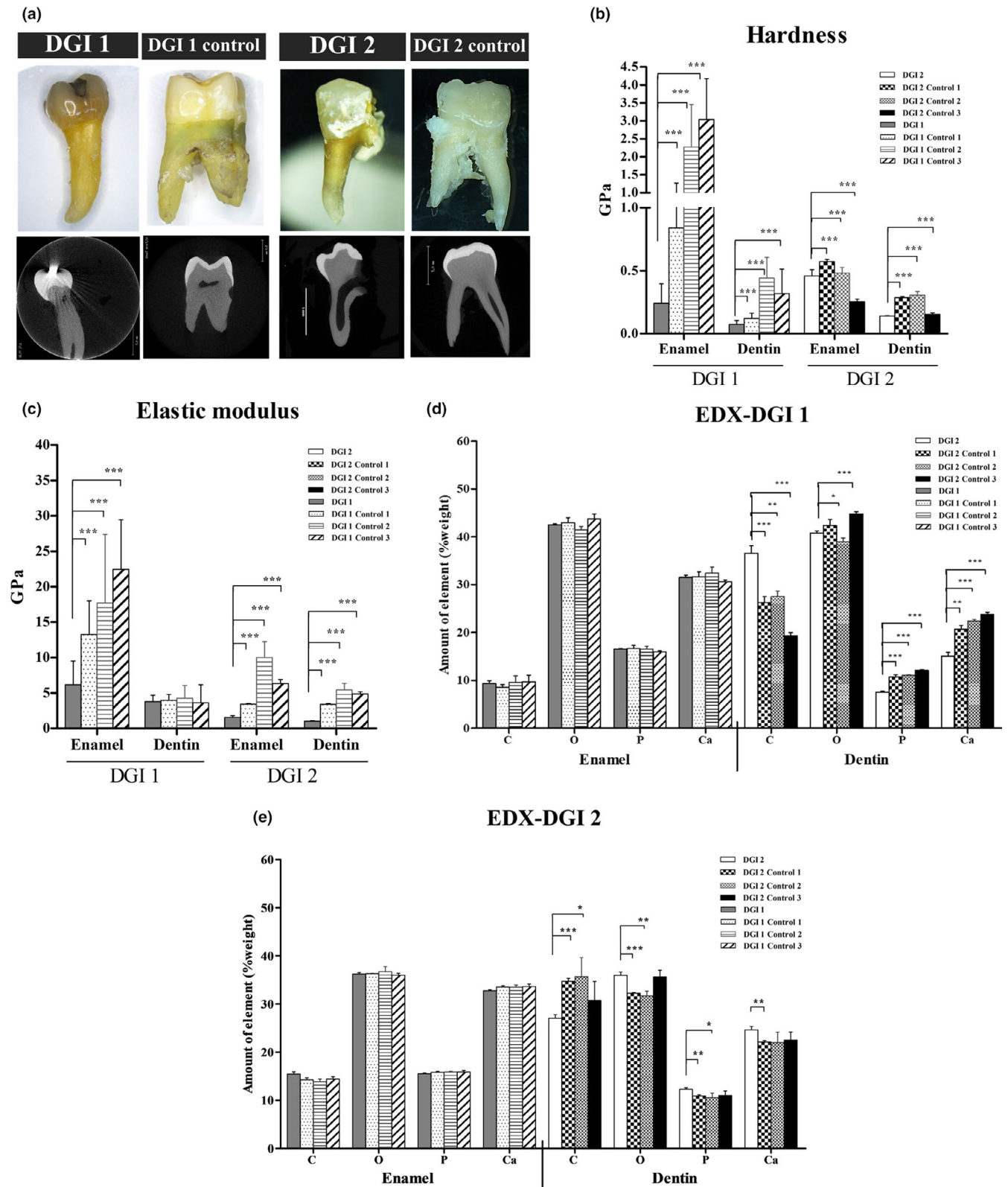


**FIGURE 4** Tooth appearance and physical properties. (a) The images and micro-CT sections of the teeth obtained from the proband (DGI1) and his son (DGI2), compared with their control teeth. (b) The dentin hardness of DGI 1 and DGI2 was significantly lower than that of the controls. (c) The elastic modulus of DGI 1 (enamel) and DGI2 (enamel and dentin) was significantly lower than that of the controls. (d, e) The mineral contents of enamel of DGI teeth were not significantly different from their controls. The calcium and phosphorous contents of DGI1 dentin were significantly lower than those of the controls whereas the DGI2 dentin contained comparable calcium and phosphorous contents to its controls. \**p* value  $\leq .05$ , \*\**p* value  $\leq .01$ , \*\*\**p* value  $\leq .001$

contrast, the dentinal tubules of the controls were circular and regularly distributed. Both DGI1 and DGI2 also showed less collagen fibers than the controls (Figure 5a–p). Moreover, the lacunae-like areas were noticeable in DGI2 dentin (Figure 5k,l). SEM also revealed that both DGI1 and DGI2 dentin had reduced number of tubules with variable diameters compared to their controls. In addition, rough peritubular and intertubular dentin consisting of ectopic calcified masses was observed in DGI teeth (Supplementary Figure 3a–d). The etched enamel of DGI teeth showed the prismatic structure comprising opened prism sheath, slight dissolution of prism core, and intact prism periphery, similar to their controls (Supplementary Figure 3e–h). The dentinoenamel junctions (DEJs) in both DGI1 and DGI2 were irregular compared to the organized interlinking junction in the controls (Supplementary Figure 3i–n).

## 4 | DISCUSSION

This study identified two Thai patients in a family who were affected with OI type IV and DGI. Both possessed two novel variants, c.752C > T (p.Ser251Phe) and c.758G > T (p.Gly253Val), in COL1A2. According to the ACMG/AMP guideline, both the p.Ser251Phe and p.Gly253Val were predicted to be likely pathogenic (Richards et al., 2015). In addition, many lines of evidence indicate the pathogenic and causative roles of the c.758G > T (p.Gly253Val) for OI. First, glycine substitutions were demonstrated to be causative of OI in a large number of cases worldwide (Budsamongkol et al., 2019; Hemwong et al., 2020; Marini et al., 2017; Udomchaiprasertkul et al., 2020). Second, the substitutions of glycine, the smallest amino acid, were shown to alter collagen structure and stability (Bhate et al., 2002; Shoulders &

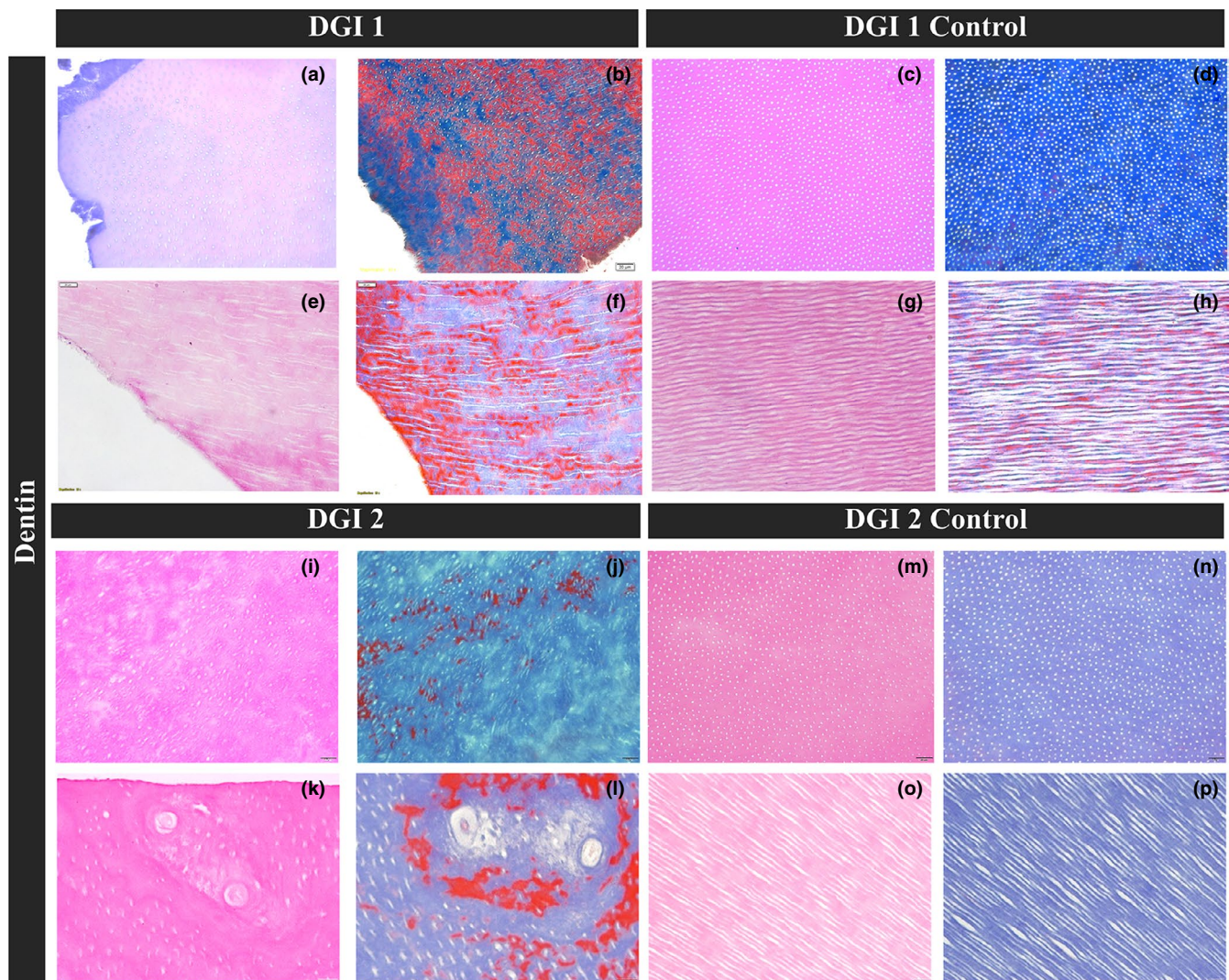


**FIGURE 5** Histological analysis. Hematoxylin and eosin staining showed irregularity, reduction, and multidirection of dentinal tubules in the dentin of DGI1 and DGI2. Masson's Trichrome staining showed inconsistent distribution of collagen (blue) in DGI dentin. Lacunae-like areas were observed in DGI2 dentin. H&E staining (x40), a, c, e, g, i, k, m, o; Masson's Trichrome (x40), b, d, f, j, l, n, p; cross sections, a, b, e, f, i, j, m, n; longitudinal sections, c, d, g, h, k, l, o, p

Raines, 2009) and the substitution of valine for glycine, in particular, was shown to undermine cross-linking of tropocollagens to form fibrils (Gautieri et al., 2009). Third, glycine substitution at the position p.Gly253, c.758G > A (p.Gly253Asp), was reported in a patient with OI (Pollitt et al., 2006). However, the pathogenic and causative role of the c.752C > T (p.Ser251Phe) for OI is not as strong as the c.758G > T (p.Gly253Val). More than 300 mutations in *COL1A2* have been identified to cause OI. Of those, only one serine substitution, c.2740A > G (p.Ser914Gly) related to OI type I is reported in the database ([www.oi.gene.le.ac.uk](http://www.oi.gene.le.ac.uk)). Although several lines of evidence suggest that the p.Ser251Phe is less pathogenic than p.Gly253Val, further studies are required to definitely conclude its pathogenicity and causality.

The distribution of glycine mutations along *COL1A2* has been associated with the phenotypes and severity of OI (Ben Amor et al., 2011; Tongkobpetch et al., 2017). Clinical features and genetic mutations of the proband and his son indicate the diagnosis of OI type IV. It has been shown that mutations in *COL1A2* are predominantly related to the non-lethal phenotype (Marini et al., 2007) and associated with OI type IV more often than Type I and III (Lin et al., 2015). Within the *COL1A2* gene, helical mutations usually lead to more severe bone phenotypes such as shorter height, lower BMD, or more disproportionate body, compared to non-helical mutations (Ben Amor et al., 2011; Liu et al., 2017; Rauch et al., 2010). In addition, the prevalence of DGI has been shown to increase when mutations occur in the C-terminal location to the p.Gly211 in the  $\alpha$ 2-chain (Lindahl et al., 2015; Maioli et al., 2019; Rauch et al., 2010). Collagen type I is a major component of extracellular matrix in dentin. Mutations of *COL1* have been shown to alter collagen structure and stability and impair function of odontoblasts (Hall et al., 2002; Shoulders & Raines, 2009). These could lead to the production of dysplastic dentin, irregular pattern and reduced number of dentinal tubules, and abnormal DEJ (Ibrahim et al., 2019; Kamasaki et al., 2019; Majorana et al., 2010). In this study, the proband and his son had short stature, low BMD, DGI, and *COL1A2* mutation. Their phenotype and genotype are in lines with previous reports.

Regarding to tooth color, both DGI1 and DGI2 showed a decrease in lightness and increase in red chroma reflecting opalescent appearance of DGI teeth. DGI1 appeared bluish while DGI2 appeared yellowish compared to their controls. Consistently, the primary tooth affected with DGI caused by *DSPP* mutation also showed an increase in red and yellow color tones (Porntaveetus, Osathanon, et al., 2018).

The hardness of DGI1 and DGI2 enamel was lower than their controls whereas their mineral contents were comparable to their controls. Similar to the enamel, the hardness of DGI1 and DGI2 dentin was significantly lower than that of their controls. DGI1 dentin showed a decrease in calcium and phosphorus contents compared with controls whereas those of DGI2 dentin were not declined. Physiologically, the chemical composition between the primary tooth and the permanent tooth is different. In addition, the calcium and phosphorus contents may be related to the age. In the enamel, calcium and phosphorus contents were significantly higher in the old age group than those in the young (He et al., 2011) while these

correlations were not observed in the dentin (Fernández-Escudero et al., 2020). Previous studies reported that pulp chambers and root canals of DGI teeth were initially abnormally large and progressively obliterated due to irregular dentin deposition (Acevedo et al., 2009; Taleb et al., 2018). Consistently, DGI1, permanent tooth of the proband age 43, showed partially obliterated pulp cavities whereas DGI2, primary tooth of the proband son age 3, showed wide pulp cavity. In addition, the lacunae-like areas were observed in DGI2 dentin. These suggest that the difference in set of teeth, age, and dentin ultrastructure could cause the difference between DGI1 and DGI2.

Enamel surface roughness values of DGI1 and DGI2 were among their controls, indicating that enamel surface of DGI teeth was unlikely to be deviated. Interestingly, we observed a significant reduction in hardness and elastic modulus of DGI1 enamel. Even though the pathology of DGI is expected occur in the dentin, the enamel-dentin formation requires reciprocal interactions of genes and signaling. In addition, the undermined dentin could cause negative impact on enamel physical properties. It was reported that the patients with OI/DGI had severe attrition and fracture of enamel (Majorana et al., 2010). Moreover, Wiczorek & Loster, 2013 demonstrated the abnormal enamel prismatic structure in DGI teeth and suggested that enamel was subject to severe attrition during mastication (Wiczorek & Loster, 2013). In this study, the ultrastructure and mineral content of DGIs' enamel were similar to controls. This implies that underlying dentin defects could contribute to the weakness of DGI enamel.

The ultrastructural investigations in the present study indicate severe pathologic change of DGI dentin. The dentinal tubules were reduced, scattered, irregular in arrangement, and variable in diameter. The collagen fibers were decreased in DGIs. These are consistent with previous reports (Hall et al., 2002; Ibrahim et al., 2019; Lindau et al., 1999; Lygidakis et al., 1996). The lacunae-like structure was also found in DGI2 dentin. In addition, the DEJs of both DGI1 and DGI2 were irregular compared to the proper interlinking line in the controls. It was suggested that a typical scallop nature of DEJ conferred a biomechanical advantage to the integrity of the tooth during mastication (Shimizu & Macho, 2007). We speculate that the irregular DEJs of DGI teeth could contribute to weak connection between enamel and dentin, making them prone to fracture.

Due to abnormal dentin and DEJ structures, DGI teeth showed the increased risk of tooth fracture, restoration failure, and periapical infection (Gallusi et al., 2006; Seow, 2003). The penetration of dental adhesives to create hybrid layer is an important factor for successful restoration of tooth-colored filling material (Nakabayashi et al., 1991). Disorganization and reduction in the number and size of dentinal tubules in DGI teeth could jeopardize the effective bonding between resin adhesives and the dentin, resulting in a consecutive failure of restorations. Abnormal dentin structure could also increase the risk of periapical lesion (Porntaveetus, Nowwarote, et al., 2018). Therefore, close monitoring of DGI patients should be implemented.

To conclude, this study demonstrated two patients affected with OI type IV and DGI. Two novel variants in *COL1A2* were identified. The DGI teeth were dark, weak, and contained abnormal dentinal

tubules and DEJ. Last but not least, this study expands phenotypic and genotypic spectra of COL1A2 mutations.

## ACKNOWLEDGEMENTS

NI was supported by Ratchadapisek Somphot Fund for Postdoctoral Fellowship, Chulalongkorn University. This project is funded by National Research Council of Thailand, Global Partnership CU-C16F630029, Health Systems Research Institute, and Thailand Research Fund (MRG6280001, DPG6180001).

## CONFLICT OF INTEREST

None to declare.

## AUTHOR CONTRIBUTION

**Narin Intarak:** Investigation; Writing-original draft. **Thunyaporn Budsamongkol:** Investigation; Writing-review & editing. **Thanakorn Theerapanon:** Data curation; Formal analysis; Writing-review & editing. **Theerapat Chanamuangkon:** Methodology; Writing-review & editing. **Anucharte Srijunbarl:** Investigation; Writing-review & editing. **Lawan Boonprakong:** Investigation; Methodology; Writing-review & editing. **Thantrira Pornraveetus:** Conceptualization; Data curation; Supervision; Writing-original draft; Writing-review & editing. **Vorasuk Shotelersuk:** Conceptualization; Resources; Visualization; Writing-review & editing.

## PEER REVIEW

The peer review history for this article is available at <https://publons.com/publon/10.1111/odi.13657>.

## ORCID

Narin Intarak  <https://orcid.org/0000-0001-7504-1403>

Thunyaporn Budsamongkol  <https://orcid.org/0000-0003-1962-2793>

Thanakorn Theerapanon  <https://orcid.org/0000-0001-6727-862X>

Theerapat Chanamuangkon  <https://orcid.org/0000-0003-0293-765X>

Anucharte Srijunbarl  <https://orcid.org/0000-0002-9199-9651>

Lawan Boonprakong  <https://orcid.org/0000-0002-5622-8691>

Thantrira Pornraveetus  <https://orcid.org/0000-0003-0145-9801>

Vorasuk Shotelersuk  <https://orcid.org/0000-0002-1856-0589>

## REFERENCES

- Acevedo, A. C., Santos, L. J. S., Paula, L. M., Dong, J., & MacDougall, M. (2009). Phenotype characterization and DSPP mutational analysis of three Brazilian dentinogenesis imperfecta type II families. *Cells Tissues Organs*, 189(1–4), 230–236. <https://doi.org/10.1159/000152917>
- Alghazali, N., Burnside, G., Moallem, M., Smith, P., Preston, A., & Jarad, F. D. (2012). Assessment of perceptibility and acceptability of color difference of denture teeth. *Journal of Dentistry*, 40(Suppl 1), e10–e17. <https://doi.org/10.1016/j.jdent.2012.04.023>
- Ben Amor, I. M., Glorieux, F. H., & Rauch, F. (2011). Genotype-phenotype correlations in autosomal dominant osteogenesis imperfecta. *Journal of Osteoporosis*, 2011, 540178. <https://doi.org/10.4061/2011/540178>

- Bhate, M., Wang, X., Baum, J., & Brodsky, B. (2002). Folding and conformational consequences of glycine to alanine replacements at different positions in a collagen model peptide. *Biochemistry*, 41(20), 6539–6547. <https://doi.org/10.1021/bi020070d>
- Budsamongkol, T., Intarak, N., Theerapanon, T., Yodsanga, S., Pornraveetus, T., & Shotelersuk, V. (2019). A novel mutation in COL1A2 leads to osteogenesis imperfecta/Ehlers-Danlos overlap syndrome with brachydactyly. *Genes and Disease*, 6(2), 138–146. <https://doi.org/10.1016/j.gendis.2019.03.001>
- Fernández-Escudero, A. C., Legaz, I., Prieto-Bonete, G., López-Nicolás, M., Maurandi-López, A., & Pérez-Cárceles, M. D. (2020). Aging and trace elements in human coronal tooth dentine. *Scientific Reports*, 10(1), 9964. <https://doi.org/10.1038/s41598-020-66472-1>
- Gallusi, G., Libonati, A., & Campanella, V. (2006). SEM-morphology in dentinogenesis imperfecta type II: Microscopic anatomy and efficacy of a dentine bonding system. *European Journal of Paediatric Dentistry*, 7(1), 9–17.
- Gautieri, A., Uzel, S., Vesentini, S., Redaelli, A., & Buehler, M. J. (2009). Molecular and mesoscale mechanisms of osteogenesis imperfecta disease in collagen fibrils. *Biophysical Journal*, 97(3), 857–865. <https://doi.org/10.1016/j.bpj.2009.04.059>
- Hall, R. K., Maniere, M. C., Palamara, J., & Hemmerle, J. (2002). Odontoblast dysfunction in osteogenesis imperfecta: An LM, SEM, and ultrastructural study. *Connective Tissue Research*, 43(2–3), 401–405. <https://doi.org/10.1080/03008200290001005>
- He, B., Huang, S., Zhang, C., Jing, J., Hao, Y., Xiao, L., & Zhou, X. (2011). Mineral densities and elemental content in different layers of healthy human enamel with varying teeth age. *Archives of Oral Biology*, 56(10), 997–1004. <https://doi.org/10.1016/j.archoralbio.2011.02.015>
- Hemwong, N., Phokaew, C., Srichomthong, C., Tongkobpetch, S., Srilanchakon, K., Supornsilchai, V., Suphapeetiporn, K., Pornraveetus, T., & Shotelersuk, V. (2020). A patient with combined pituitary hormone deficiency and osteogenesis imperfecta associated with mutations in LHX4 and COL1A2. *Journal of Advanced Research*, 21, 121–127. <https://doi.org/10.1016/j.jare.2019.10.006>
- Ibrahim, S., Strange, A. P., Aguayo, S., Shinawi, A., Harith, N., Mohamed-Ibrahim, N., & Bozec, L. (2019). Phenotypic properties of collagen in dentinogenesis imperfecta associated with osteogenesis imperfecta. *International Journal of Nanomedicine*, 14, 9423–9435. <https://doi.org/10.2147/IJN.S217420>
- Jagadeesh, K. A., Wenger, A. M., Berger, M. J., Guturu, H., Stenson, P. D., Cooper, D. N., Bernstein, J. A., & Bejerano, G. (2016). M-CAP eliminates a majority of variants of uncertain significance in clinical exomes at high sensitivity. *Nature Genetics*, 48(12), 1581–1586. <https://doi.org/10.1038/ng.3703>
- Kamasaki, Y., Imamura, K., Nishimata, H., Nishiguchi, M., & Fujiwara, T. (2019). Study of enamel and dentin in primary teeth with dentinogenesis imperfecta type I: A case report. *Journal of Dental Research and Reports*, 2, 1–4. <https://doi.org/10.15761/JDRR.1000110>
- Li, Q., & Wang, K. (2017). InterVar: Clinical interpretation of genetic variants by the 2015 ACMG-AMP guidelines. *American Journal of Medical Genetics*, 100(2), 267–280. <https://doi.org/10.1016/j.ajhg.2017.01.004>
- Lin, H. Y., Chuang, C. K., Su, Y. N., Chen, M. R., Chiu, H. C., Niu, D. M., & Lin, S. P. (2015). Genotype and phenotype analysis of Taiwanese patients with osteogenesis imperfecta. *Orphanet Journal of Rare Diseases*, 10, 152. <https://doi.org/10.1186/s13023-015-0370-2>
- Lindahl, K., Astrom, E., Rubin, C. J., Grigelioniene, G., Malmgren, B., Ljunggren, O., & Kindmark, A. (2015). Genetic epidemiology, prevalence, and genotype-phenotype correlations in the Swedish population with osteogenesis imperfecta. *European Journal of Human Genetics*, 23(8), 1042–1050. <https://doi.org/10.1038/ejhg.2015.81>
- Lindau, B. M., Dietz, W., Hoyer, I., Lundgren, T., Storhaug, K., & Noren, J. G. (1999). Morphology of dental enamel and

- dentine-enamel junction in osteogenesis imperfecta. *International Journal of Paediatric Dentistry*, 9(1), 13–21. <https://doi.org/10.1046/j.1365-263x.1999.00101.x>
- Lindert, U., Cabral, W. A., Ausavarat, S., Tongkobpetch, S., Ludin, K., Barnes, A. M., Yeetong, P., Weis, M., Krabichler, B., Srichomthong, C., Makareeva, E. N., Janecke, A. R., Leikin, S., Röthlisberger, B., Rohrbach, M., Kennerknecht, I., Eyre, D. R., Suphapeetiporn, K., Giunta, C., ... Shotelersuk, V. (2016). MBTPS2 mutations cause defective regulated intramembrane proteolysis in X-linked osteogenesis imperfecta. *Nature Communications*, 7, 11920. <https://doi.org/10.1038/ncomms11920>
- Liu, Y., Asan, Ma, D., Lv, F., Xu, X., Wang, J., Xia, W., Jiang, Y., Wang, O., Xing, X., Yu, W., Wang, J., Sun, J., Song, L., Zhu, Y., Yang, H., Wang, J., & Li, M. (2017). Gene mutation spectrum and genotype-phenotype correlation in a cohort of Chinese osteogenesis imperfecta patients revealed by targeted next generation sequencing. *Osteoporosis International*, 28(10), 2985–2995. <https://doi.org/10.1007/s00198-017-4143-8>
- Lygidakis, N. A., Smith, R., & Oulis, C. J. (1996). Scanning electron microscopy of teeth in osteogenesis imperfecta type I. *Oral Surgery, Oral Medicine, Oral Pathology and Oral Radiology*, 81(5), 567–572. [https://doi.org/10.1016/S1079-2104\(96\)80048-5](https://doi.org/10.1016/S1079-2104(96)80048-5)
- Maioli, M., Gnoli, M., Boarini, M., Tremosini, M., Zambrano, A., Pedrini, E., Mordenti, M., Corsini, S., D'Eufemia, P., Versacci, P., Celli, M., & Sangiorgi, L. (2019). Genotype-phenotype correlation study in 364 osteogenesis imperfecta Italian patients. *European Journal of Medical Genetics*, 27(7), 1090–1100. <https://doi.org/10.1038/s41431-019-0373-x>
- Majorana, A., Bardellini, E., Brunelli, P. C., Lacaíta, M., Cazzolla, A. P., & Favia, G. (2010). Dentinogenesis imperfecta in children with osteogenesis imperfecta: A clinical and ultrastructural study. *International Journal of Paediatric Dentistry*, 20(2), 112–118. <https://doi.org/10.1111/j.1365-263X.2010.01033.x>
- Marini, J. C., Forlino, A., Bächinger, H. P., Bishop, N. J., Byers, P. H., Paepe, A. D., Fassier, F., Fratzl-Zelman, N., Kozloff, K. M., Krakow, D., Montpetit, K., & Semler, O. (2017). Osteogenesis imperfecta. *Nature Reviews Disease Primers*, 3, 17052. <https://doi.org/10.1038/nrdp.2017.52>
- Marini, J. C., Forlino, A., Cabral, W. A., Barnes, A. M., San Antonio, J. D., Milgrom, S., Hyland, J. C., Körkkö, J., Prockop, D. J., De Paepe, A., Coucke, P., Symoens, S., Glorieux, F. H., Roughley, P. J., Lund, A. M., Kuurila-Svahn, K., Hartikka, H., Cohn, D. H., Krakow, D., ... Byers, P. H. (2007). Consortium for osteogenesis imperfecta mutations in the helical domain of type I collagen: Regions rich in lethal mutations align with collagen binding sites for integrins and proteoglycans. *Human Mutation*, 28(3), 209–221. <https://doi.org/10.1002/humu.20429>
- Nakabayashi, N., Nakamura, M., & Yasuda, N. (1991). Hybrid layer as a dentin-bonding mechanism. *Journal of Esthetic and Restorative Dentistry*, 3(4), 133–138. <https://doi.org/10.1111/j.1708-8240.1991.tb00985.x>
- Ng, P. C., & Henikoff, S. (2003). SIFT: Predicting amino acid changes that affect protein function. *Nucleic Acids Research*, 31(13), 3812–3814. <https://doi.org/10.1093/nar/gkg509>
- O'Connell, A. C., & Marini, J. C. (1999). Evaluation of oral problems in an osteogenesis imperfecta population. *Oral Surgery, Oral Medicine, Oral Pathology and Oral Radiology*, 87(2), 189–196. [https://doi.org/10.1016/S1079-2104\(99\)70272-6](https://doi.org/10.1016/S1079-2104(99)70272-6)
- Pollitt, R., McMahon, R., Nunn, J., Bamford, R., Afifi, A., Bishop, N., & Dalton, A. (2006). Mutation analysis of COL1A1 and COL1A2 in patients diagnosed with osteogenesis imperfecta type I-IV. *Human Mutation*, 27(7), 716. <https://doi.org/10.1002/humu.9430>
- Porntaveetus, T., Nowwarote, N., Osathanon, T., Theerapanon, T., Pavasant, P., Boonprakong, L., Sanon, K., Srisawasdi, S., Suphapeetiporn, K., & Shotelersuk, V. (2018). Compromised alveolar bone cells in a patient with dentinogenesis imperfecta caused by DSPP mutation. *Clinical Oral Investigations*, 23(1), 303–313. <https://doi.org/10.1007/s00784-018-2437-7>
- Porntaveetus, T., Osathanon, T., Nowwarote, N., Pavasant, P., Srichomthong, C., Suphapeetiporn, K., & Shotelersuk, V. (2018). Dental properties, ultrastructure, and pulp cells associated with a novel DSPP mutation. *Oral Diseases*, 24(4), 619–627. <https://doi.org/10.1111/odi.12801>
- Rauch, F., Lalic, L., Roughley, P., & Glorieux, F. H. (2010). Genotype-phenotype correlations in nonlethal osteogenesis imperfecta caused by mutations in the helical domain of collagen type I. *European Journal of Human Genetics*, 18(6), 642–647. <https://doi.org/10.1038/ejhg.2009.242>
- Richards, S., Aziz, N., Bale, S., Bick, D., Das, S., Gastier-Foster, J., Grody, W. W., Hegde, M., Lyon, E., Spector, E., Voelkerding, K., & Rehm, H. L. (2015). Standards and guidelines for the interpretation of sequence variants: A joint consensus recommendation of the American College of Medical Genetics and Genomics and the Association for Molecular Pathology. *Genetics in Medicine*, 17(5), 405–424. <https://doi.org/10.1038/gim.2015.30>
- Seow, W. K. (2003). Diagnosis and management of unusual dental abscesses in children. *Australian Dental Journal*, 48(3), 156–168. <https://doi.org/10.1111/j.1834-7819.2003.tb00026.x>
- Shimizu, D., & Macho, G. A. (2007). Functional significance of the microstructural detail of the primate dentino-enamel junction: A possible example of exaptation. *Journal of Human Evolution*, 52(1), 103–111. <https://doi.org/10.1016/j.jhevol.2006.08.004>
- Shoulders, M. D., & Raines, R. T. (2009). Collagen structure and stability. *Annual Review of Biochemistry*, 78(1), 929–958. <https://doi.org/10.1146/annurev.biochem.77.032207.120833>
- Sillence, D. O., Senn, A., & Danks, D. M. (1979). Genetic heterogeneity in osteogenesis imperfecta. *Journal of Medical Genetics*, 16(2), 101–116. <https://doi.org/10.1136/jmg.16.2.101>
- Taleb, K., Lauridsen, E., Daugaard-Jensen, J., Nieminen, P., & Kreiborg, S. (2018). Dentinogenesis imperfecta type II- genotype and phenotype analyses in three Danish families. *Molecular Genetics & Genomic Medicine*, 6(3), 339–349. <https://doi.org/10.1002/mgg3.375>
- Tongkobpetch, S., Limpaphayom, N., Sangsin, A., Porntaveetus, T., Suphapeetiporn, K., & Shotelersuk, V. (2017). A novel de novo COL1A1 mutation in a Thai boy with osteogenesis imperfecta born to consanguineous parents. *Genetics and Molecular Biology*, 40(4), 763–767. <https://doi.org/10.1590/1678-4685-GMB-2016-0033>
- Udomchaiprasertkul, W., Kuptanon, C., Porntaveetus, T., & Shotelersuk, V. (2020). A family with homozygous and heterozygous p.Gly337Ser mutations in COL1A2. *European Journal of Medical Genetics*, 63(6), 103896. <https://doi.org/10.1016/j.ejmg.2020.103896>
- Wieczorek, A., & Loster, J. (2013). Dentinogenesis imperfecta type II: Ultrastructure of teeth in sagittal sections. *Folia Histochemica et Cytobiologica*, 51(3), 244–247. <https://doi.org/10.5603/FHC.2013.0035>
- Yamanel, K., Caglar, A., Ozcan, M., Gulsah, K., & Bagis, B. (2010). Assessment of color parameters of composite resin shade guides using digital imaging versus colorimeter. *Journal of Esthetic and Restorative Dentistry*, 22(6), 379–388. <https://doi.org/10.1111/j.1708-8240.2010.00370.x>

## SUPPORTING INFORMATION

Additional supporting information may be found online in the Supporting Information section.

**How to cite this article:** Intarak N, Budsamongkol T, Theerapanon T, et al. Tooth ultrastructure of a novel COL1A2 mutation expanding its genotypic and phenotypic spectra. *Oral Dis*. 2020;00:1–11. <https://doi.org/10.1111/odi.13657>